Microscopic bath effects on noise spectra in semiconductor quantum dot qubits

Seongjin Ahn,[1] S. Das Sarma,[1] and J. P. Kestner[2,*]

[1] *Condensed Matter Theory Center and Joint Quantum Institute, Department of Physics, University of Maryland College Park, MD 20742, USA*

[2] *Department of Physics, University of Maryland Baltimore County, Baltimore, MD 21250, USA*

When a system is thermally coupled to only a small part of a larger bath, statistical fluctuations of the temperature (more precisely, the internal energy) of this "sub-bath" around the mean temperature defined by the larger bath can become significant. We show that these temperature fluctuations generally give rise to 1/f-like noise power spectral density from even a single two-level system. We extend these results to a distribution of fluctuators, finding the corresponding modification to the Dutta-Horn relation. Then we consider the specific situation of charge noise in silicon quantum dot qubits and show that recent experimental data [1] can be modeled as arising from as few as two two-level fluctuators, and accounting for sub-bath size improves the quality of the fit.

Charge noise, particularly the so-called 1/f noise ubiquitous in electronic devices, is currently the most significant roadblock to the successful development of semiconductor-based scalable solid state qubits. It is well known that an ensemble of thermally activated two-level fluctuators (TLFs) with a broad range of switching rates gives rise to a 1/f power spectral density (PSD) with a linear temperature dependence [2]. This is the standard hand-waving explanation given to explain wide-spread observations of pink noise in solid state qubit devices, with some sort of charged defects playing the role of the TLFs. Early data from laterally-defined quantum dots in silicon showed that the noise power indeed appears to increase with temperature [3], but with large error bars that preclude a more detailed conclusion. Recent experiments, however, have shown striking deviation from the expected linear temperature dependence. Ref. [1] measures a temperature dependence which is not only nonlinear, but in some cases *non-monotonic*, qualitatively consistent with the Dutta-Horn model [4] of a large ensemble of TLFs with a non-uniform distribution of switching rates, although any expected quantitative consistency varies widely within the data set. Meanwhile, Ref. [5] finds a quadratic temperature dependence. On the other hand, Ref. [6] observes a T_2^* decoherence time that is approximately *constant* over a range of temperatures from 0.45K-1.2K, suggesting that their charge noise comes from a few TLFs with activation energies much smaller than k_BT, rather than a broad distribution. The situation, particularly in the measured noise temperature dependence, is thus quite confusing.

In this work we show that, in principle, 1/f noise with nonlinear temperature dependence can be produced by even a single TLF coupled to a small subsection of the thermal bath. Although we cannot assert that our proposed mechanism is operational in semiconductor qubits (in fact, the physical mechanism underlying 1/f noise is still obscure), we show that the experimental data of Ref. [1] can be reasonably fit as arising from a small number of TLFs, and that the fit is improved by incorporating this microscopic thermal bath effect via an additional fit parameter.

The essential narrative here is that, even within the TLF model, observation of 1/f noise over some broad frequency range need not imply an ensemble of TLFs. One (or few) TLFs can suffice, in which case a nonlinear temperature dependence is natural. This conclusion of the adequacy of just a few TLFs obviously has important implications.

We assume a stochastic TLF with activation energy E and a thermally activated transition time $\tau \exp(E/k_BT_{sb})$. Here we take T_{sb} to be the effective temperature of the microscopic portion of the thermal bath to which the fluctuator is coupled (i.e., the "sub-bath"). T_{sb} is then a stochastically fluctuating quantity whose average is the same as the macroscopic bath temperature, T, but with variance

$$\sigma_{sb}^2 = \frac{k_BT^2}{C_V} \tag{1}$$

where C_V is the heat capacity of the microscopic sub-bath. Since C_V is an extrinsic quantity, σ_{sb} is proportional to one over the square root of the volume of the sub-bath. However, it is quite physical to assume that a microscopic two-level fluctuator may be coupled to only a microscopic sub-bath, so the variance could be non-negligible. For instance, in semiconductor quantum dots one typically imagines the charge noise as arising from charged TLFs coupled via Coulomb interaction to a thermal electrostatic environment, but since the Coulomb interaction is screened by the nearby two-dimensional electron gas (2DEG) and the dense array of metallic top gates, each TLF will only interact strongly with its immediate surroundings. Generally, C_V is also a function of T; at low temperatures, it is dominated by the electronic heat capacity, which is linear in T. For example, considering a 2DEG sub-bath of area A, the variance is

$$\sigma_{sb}^2 = \frac{3\hbar^2T}{\pi m A k_B}, \tag{2}$$

where m is the effective mass of the electrons. This can certainly be non-negligible, since for Si, with an effective

mass of $m = 0.19m_e$ (where m_e is the electron mass), and an area of one square micron, at a typical temperature of 50 mK one would have sub-bath fluctuations of 14 mK.

Averaging over the sub-bath statistical temperature distribution $f(T_{sb})$, the PSD is

$$S(\omega) = \Delta^2 \int_{-\infty}^{\infty} dT_{sb} f(T_{sb}) \frac{4\tau \exp\left(E/k_B T_{sb}\right)}{1+\omega^2\tau^2 \exp\left(2E/k_B T_{sb}\right)}$$
$$= \frac{2\Delta^2}{\omega} \int_{-\infty}^{\infty} dT_{sb} f(T_{sb}) \mathrm{sech}\left(\frac{E}{k_B T_{sb}} + \ln(\omega\tau)\right), \quad (3)$$

where Δ^2 is the total variance of the signal produced by the switching events. For convenience, we will integrate over a normal distribution of temperatures,

$$S(\omega) = \frac{2\Delta^2}{\omega\sqrt{2\pi}\sigma_{sb}} \int_{-\infty}^{\infty} dT_{sb} e^{-\frac{(T_{sb}-T)^2}{2\sigma_{sb}^2}} \mathrm{sech}\left(\frac{E}{k_B}\left(\frac{1}{T} - \frac{1}{T_\omega}\right)\right), \quad (4)$$

where we have also defined

$$T_\omega \equiv \frac{E}{k_B \ln \frac{1}{\omega\tau}}. \quad (5)$$

Note that we implicitly assume that $\sigma_{sb} < T$, with unphysical negative sub-bath temperatures nonetheless permitted in the tail of the distribution. That can trivially be remedied by truncating the distribution on the lower side, but that produces more complicated expressions without affecting the conclusions below (see Supplementary Information).

The integrand in Eq. (4) contains two peaks, one at the distribution's mean, T, and one from the Lorentzian at T_ω. While the integral is easily carried out numerically for any set of parameters, the qualitative behavior is illuminated by the following approximation. Assuming the peaks are well separated, approximate the sech term as a constant in the vicinity of T and as a gaussian in the vicinity of T_ω, with width

$$\sigma_\omega \equiv \frac{E}{k_B \ln^2 \frac{1}{\omega\tau}}, \quad (6)$$

so as to obtain

$$S(\omega) \approx \frac{2\Delta^2}{\omega} \mathrm{sech}\left(\frac{E}{k_B}\left(\frac{1}{T_{sb}} - \frac{1}{T_\omega}\right)\right) + \frac{2\Delta^2}{\omega} \frac{\sigma_\omega}{\sqrt{\sigma_{sb}^2 + \sigma_\omega^2}} e^{-\frac{(T-T_\omega)^2}{2(\sigma_{sb}^2+\sigma_\omega^2)}}. \quad (7)$$

This has nontrivial frequency and temperature dependence, but in the low-frequency limit $T_\omega \ll T$ and $\sigma_\omega \ll \sigma_{sb}$,

$$S(\omega) \approx \frac{4\tau\Delta^2}{1+\omega^2\tau^2} + \frac{2E\Delta^2}{k_B \sigma_{sb} \omega \ln^2 \frac{1}{\omega\tau}} e^{-\frac{(T-T_\omega)^2}{2\sigma_{sb}^2}}. \quad (8)$$

The first term is the typical Lorentzian spectrum of a single TLF. The second term rises above this Lorentzian floor at low frequencies as $1/\omega \ln^2 \omega\tau$, which over a broad frequency range centered around ω_0 is practically indistinguishable from $1/\omega^\alpha$ with $\alpha = 1 + 2/\ln \omega_0\tau$. An example of this behavior is shown in Fig. 1.

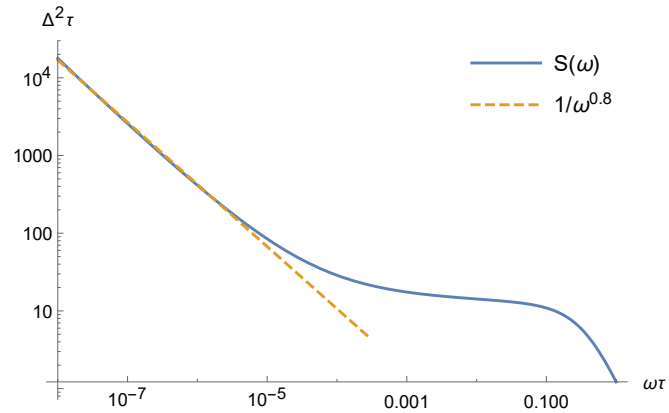

FIG. 1: Power spectral density vs frequency from Eq. (4) for $\frac{E}{k_B T} = 1$, $\frac{\sigma_{sb}}{T} = 0.3$.

Thus, if temperature fluctuations are significant, one can expect to find $1/\omega^\alpha$ noise at frequencies below roughly

$$\omega_{1/\mathrm{f}} \sim 0.01\tau^{-1} \frac{E}{2k_B\sigma_{sb}} \exp\left(-\frac{T^2}{2\sigma_{sb}^2}\right), \quad (9)$$

transitioning to white noise at intermediate frequencies, and finally falling as $1/\omega^2$ at frequencies above τ^{-1}. Although no quantum dot experiment to our knowledge has measured the noise spectrum at high enough frequency to conclusively observe the roll-off to $1/\omega^2$ (although Ref. [7] finds suggestions of it in the data of Ref. [8]), some have observed a whitening of $1/\omega^\alpha$ noise with increasing frequency [1, 9].

Turning our attention now to the temperature dependence, we can compute Eq. (4) numerically for a given set of parameters, as shown in Fig. 2. The PSD is peaked around T_ω and is qualitatively similar to the PSD in the absence of temperature fluctuations. It is instructive to look at the limiting cases analytically. At temperatures well above T_ω, Eq. (8) holds, so one has an exponential decay to a constant value as temperature increases. This is the same high-temperature dependence as in the absence of fluctuations. The data in Ref. [6] is believed to correspond to this constant, high-temperature tail. For $T < T_\omega$ (and hence also $< E/k_B$), the peaks of the integrand in Eq. (4) at T and T_ω are no longer well separated. However, by approximating the sech as a decaying exponential (i.e., neglecting unity in the denominator of Eq. (3) compared to the exponentially large term), we

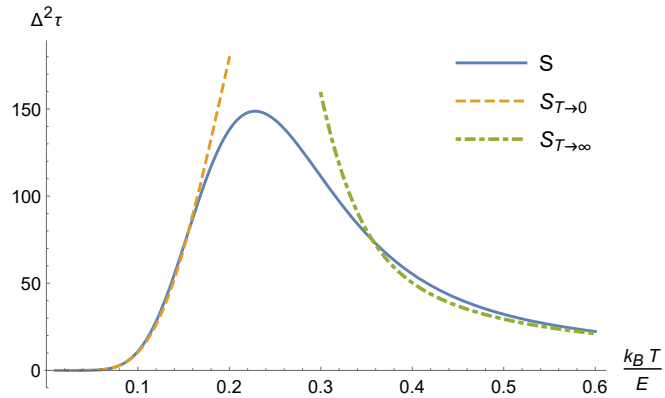

FIG. 2: Power spectral density at $\omega\tau = 0.01$ vs temperature for $\frac{k_B\sigma_{sb}}{E} = 0.1\sqrt{k_BT/E}$. The solid line is numerically computed from from Eq. (4), the dashed line is from Eq. (12), and the dotted line is from Eq. (8).

can make a gaussian approximation to the integrand

$$S(\omega) \overset{T\to 0}{\approx} \frac{4\Delta^2}{\omega^2\tau}\frac{1}{\sqrt{2\pi}\sigma_{sb}}\int_{-\infty}^{\infty} dT_{sb} e^{-\frac{E}{k_BT_{sb}}-\frac{(T_{sb}-T)^2}{2\sigma_{sb}^2}}$$
$$\approx \frac{4\Delta^2}{\omega^2\tau}\frac{e^{-\frac{E}{k_BT_*}-\frac{(T_*-T)^2}{2\sigma_*^2}}}{\sqrt{2\pi}\sigma_{sb}}\int_{-\infty}^{\infty} dT_{sb} e^{-\frac{(T_{sb}-T_*)^2}{2\sigma_*^2}}, \quad (10)$$

where the expressions for T_* and σ_* in terms of the physical parameters are algebraically cumbersome, but simplify in the low-temperature limit if we assume $\lim_{T\to 0} T/\left(\sigma_{sb}^2 E/k_B\right)^{1/3} = 0$ (as is the case for electrons (2)) to

$$T_* = \frac{1}{3}T + \left(\frac{E}{k_B}\sigma_{sb}^2\right)^{1/3}, \qquad \sigma_* = \frac{1}{\sqrt{3}}\sigma_{sb}. \quad (11)$$

So one obtains

$$S(\omega) \overset{T\to 0}{\approx} \frac{4\sqrt{2}\Delta^2}{\sqrt{3}\omega^2\tau}\exp\left(-\frac{1}{2}\left(-\frac{2T}{3\sigma_{sb}}+\left(\frac{E}{k_B\sigma_{sb}}\right)^{1/3}\right)^2\right)$$
$$\times \exp\left(-\frac{3E/k_B}{T+3\left(\sigma_{sb}^2E/k_B\right)^{1/3}}\right). \quad (12)$$

So, instead of the typical linear temperature dependence [2], it is exponentially flat at low temperatures, going like $\exp\left(-\left(\frac{3\sqrt{\pi m A}E}{2\sqrt{2k_B}\hbar}\right)^{2/3}T^{-1/3}\right)$.

This flatness at low temperatures is qualitatively consistent with some of the data sets of Ref. [1], and we show below that superposing PSDs as in Fig. 2 of a few TLFs with different activation energies can provide an alternate way to understand and fit the nonlinear behavior in Ref. [1]. However, at this point it suffices to note that by dropping the assumption that 1/f noise must imply a continuous distribution of TLFs, we have preserved the nonlinear temperature dependence of a single TLF, and, depending on the parameter values, one could obtain seemingly very different behaviors if one observes over only a narrow range of temperatures.

We now discuss briefly how the PSD of a continuous distribution of TLFs would be affected by sub-bath temperature fluctuations. The classic Dutta-Horn model [4] for a temperature-independent distribution of activation energies, $F(E)$, gives

$$S = \frac{2\pi k_BT}{\omega}F\left(E_\omega\right), \quad (13)$$

where $E_\omega \equiv k_BT\ln\frac{1}{\omega\tau}$, in which case the frequency dependence and the temperature dependence are linked as

$$\gamma \equiv -\frac{\partial\ln S}{\partial\ln\omega} = 1 - \frac{1}{\ln\omega\tau}\left(\frac{\partial\ln S}{\partial\ln T}-1\right). \quad (14)$$

Modifying Eq. (13) to the case of a fluctuating sub-bath temperature (more precisely, starting from Eq. (3) and assuming F is broad, with a width much larger than k_BT such that the sech function can be approximated as a delta function),

$$S = \frac{\sqrt{2\pi}k_B}{\omega\sigma_{sb}}\int_{-\infty}^{\infty} dT_{sb}T_{sb}F(kT_{sb}\ln\frac{1}{\omega\tau})\exp\left(-\frac{(T-T_{sb})^2}{2\sigma_{sb}^2}\right). \quad (15)$$

Since the distribution of activation energies is assumed narrow compared to the distribution of sub-bath temperatures, we can do the integration in Eq. (15) by approximating

$$T_{sb}F(k_BT_{sb}\ln\frac{1}{\omega\tau}) \approx TF\left(E_\omega\right)$$
$$+\left(F\left(E_\omega\right)+E_\omega F'\left(E_\omega\right)\right)\left(T_{sb}-T\right)$$
$$+\left(\frac{E_\omega}{T}F'\left(E_\omega\right)+\frac{E_\omega^2}{2T}F''\left(E_\omega\right)\right)\left(T_{sb}-T\right)^2. \quad (16)$$

Plugging this into Eq. (15) yields

$$S(\omega) = \frac{2\pi k_BT}{\omega}F\left(E_\omega\right)$$
$$+\frac{\pi k_B^2\sigma_{sb}^2}{\omega}\left[2\ln\frac{1}{\omega\tau}F'\left(E_\omega\right)+E_\omega\ln\frac{1}{\omega\tau}F''\left(E_\omega\right)\right]. \quad (17)$$

Then it is straightforward to obtain the corresponding approximate modified Dutta-Horn relationship:

$$\gamma = 1 - \frac{1}{\ln \omega\tau}\left(\frac{\partial \ln S}{\partial \ln T} - 1\right)\left(1 + \frac{2\sigma_{sb}^2\left(2F'\left(E_\omega\right) + E_\omega F''\left(E_\omega\right)\right)}{2\left(T^2 - \sigma_{sb}^2\right)F'\left(E_\omega\right) + E_\omega\sigma_{sb}^2\left(2F''\left(E_\omega\right) + E_\omega F'''\left(E_\omega\right)\right)}\right). \tag{18}$$

The main point here is that including temperature fluctuations destroys the key feature of the Dutta-Horn result that the relationship between the frequency dependence and temperature dependence is independent of the details of the activation energy distribution. Only in the restricted case of negligible second- and higher-order derivatives of F does the relationship becomes independent of the form of F:

$$\gamma = 1 - \frac{1}{\ln\left(\omega\tau\right)}\left(\frac{\partial \ln S}{\partial \ln T} - 1\right)\frac{1 + \sigma_{sb}^2/T^2}{1 - \sigma_{sb}^2/T^2}. \tag{19}$$

Generally, the frequency and temperature dependences are now decoupled in the sense that one cannot predict one from the other without knowing the underlying distribution. In such a scenario, the details of the noise would matter a great deal leading possibly to nonuniversal experimental behavior.

We now turn to the experimental data of Ref. [1]. There the charge noise in several silicon double quantum dots was measured as a function of temperature at 1 Hz, as well as the local frequency dependence exponent, γ. We find that the data can be described reasonably well with our theory using as few as two discrete TLFs,

$$\sum_{i=1}^{2}\frac{\Delta_i^2\sqrt{2mAk_B}}{\hbar\omega\sqrt{3T}}\int_{-\infty}^{\infty}dT_{sb}e^{-\frac{(T_{sb}-T)^2}{\frac{6\hbar^2 T}{\pi m A k_B}}}\,\mathrm{sech}\left(\frac{E_i}{k_B T_{sb}} + \ln(\omega\tau_i)\right) \tag{20}$$

by fitting over the switching times (τ_i), activation energies (E_i), and fluctuator strengths (Δ_i^2), as well as a common 2D sub-bath area (A), where we have made the physically reasonable assumption that the heat capacity of the thermal bath is dominated by the electronic contribution and used Eq. (2). The objective function simultaneously minimizes net deviations from the moving average of the noisy S and γ data with equal weighting, and the minimization is carried out via a local gradient search using the *fmincon* function in Matlab. The fitting parameters are constrained to lie within $0 - 10$ s for τ, $0{-}100$ meV for E_i, $0{-}10^4$ meV^2 for Δ_i^2, and 2nm-100μm for $\sqrt{A/\pi}$ when it is finite. In the infinite sub-bath case, $A \to \infty$, the temperature distribution corresponds to a delta function.

In Fig. 3 we show an example of the results of the fitting with and without taking a microscopic sub-bath area. (Fits to the complete data set are included in the Supplementary Information.) Even the fit using an infinite thermal sub-bath appears better than the standard Dutta-Horn results, although this happens because we are just fitting S (a function of T and ω) over a cut at constant ω while also fitting the derivative $\partial_\omega S$ perpendicular to the cut. As we showed at the outset, incorporating a microscopic sub-bath area in principle allows for a $1/\omega$-type frequency dependence over the whole plane. Even restricting ourselves to the data in hand, there is a noticeable improvement in the fit when including the effects of a microscopic sub-bath. It is interesting that the sub-bath sizes that emerge from the fit are quite consistent across different dots and correspond to disks with radii of about 100 nm, which is physically reasonable for these devices. The data can be fit more closely with three or four TLFs (see Supplemental Information), but given how much variance the data displays, it does not make sense to strive for too much precision in fitting the average.

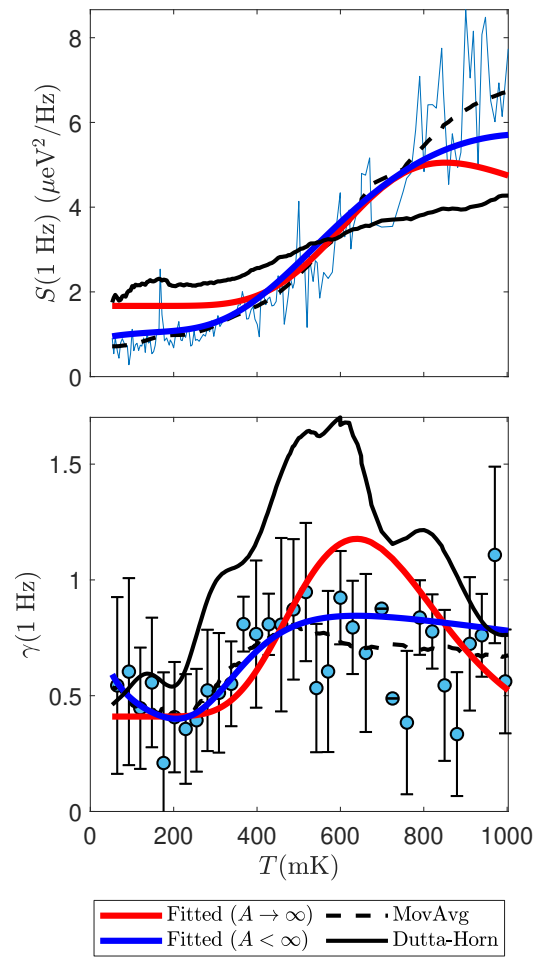

FIG. 3: Data from Supplementary Fig. 2b and d of Ref. [1] (Device 1, QD R1, Right), along with fits using only two fluctuators. The fitting parameters are given in Table I.

One ramification of having only a few relevant TLFs

	Parameter	Fluctuator 1	Fluctuator 2
$A \to \infty$	τ (ms)	8.397	80.803
	E (meV)	0.216	5.414×10^{-11}
	Δ_i^2 (meV^2)	2.688	1.644
$A < \infty$	τ (ms)	3.843×10^{-5}	52.743
	E (meV)	1.518	4.104×10^{-3}
	Δ_i^2 (meV^2)	21.899	1.529
	$\sqrt{A/\pi}$ (nm)	68.855 nm	

TABLE I: Fitting parameter values for Fig. 3.

would be that increasing temperature may not be as deleterious to coherence as it is for typical $1/f$ noise, as suggested in Ref. [6]. If it is furthermore true that these TLFs are indeed coupled to a microscopic sub-bath with appreciable temperature fluctuations, it could have some other surprising but testable ramifications. For instance, it is natural to wonder what happens if the sub-bath is small enough that the effective temperature distribution has a long tail leading to fluctuations larger than the mean temperature. Indeed, for a simple planar bath where there is no other relevant length scale, the sub-bath area should go like the square of the distance, d, between the TLF and the bath, so the critical distance at which $\sigma_{sb} \sim T$ is $d_c \sim \hbar/\sqrt{mk_BT}$, which is around 200nm for $T \sim 100$mK in Si. The dependence of the low-frequency PSD amplitude on the distance goes like $\sim d \exp\left(-d^2 k_B T m/\hbar^2\right)$ (cf. Eqs. (8) and (2)), which diminishes linearly with decreasing distance below d_c before saturating at the Lorentzian floor. Thus, one has the counterintuitive possibility of suppressing low-frequency noise by bringing the thermal electronic bath (presumably the capacitively coupled surrounding 2DEG, or the metal gates) in *closer* contact with the TLFs (perhaps charged defects at the oxide interface, or near the semiconductor surface).

In conclusion, we have shown how a $1/f$ noise power spectral density (PSD) with nonlinear temperature dependence, often modeled as arising from a broad distribution of two-level fluctuators (TLFs) via the Dutta-Horn relation, can in fact emerge from even one or two TLFs when coupled to a microscopic thermal sub-bath due to effective temperature fluctuations. If a broad distribution of TLFs is coupled to such a bath, the strict connection between local frequency and temperature scalings enforced by the Dutta-Horn relation is relaxed. Finally, we noted that recent experimental measurements of both the local frequency scaling and a nonlinear temperature dependence in silicon quantum dots can be reasonably explained as arising from as few as two TLFs.

The authors thank Elliot Connors for providing the data sets measured in Ref. [1]. SA and SDS acknowledge support by the Laboratory for Physical Sciences. JPK acknowledges support by the Army Research Office (ARO) under Grant Number W911NF-17-1-0287.

* jkestner@umbc.edu

[1] E. J. Connors, J. Nelson, H. Qiao, L. F. Edge, and J. M. Nichol, Phys. Rev. B **100**, 165305 (2019).
[2] S. Kogan, *Electronic Noise and Fluctuations in Solids* (Cambridge University Press, 1996), ISBN 0521460344.
[3] B. M. Freeman, J. S. Schoenfield, and H. Jiang, Appl. Phys. Lett. **108**, 253108 (2016).
[4] P. Dutta, P. Dimon, and P. M. Horn, Phys. Rev. Lett. **43**, 646 (1979).
[5] L. Petit, J. M. Boter, H. G. J. Eenink, G. Droulers, M. L. V. Tagliaferri, R. Li, D. P. Franke, K. J. Singh, J. S. Clarke, R. N. Schouten, et al., Phys. Rev. Lett. **121**, 076801 (2018).
[6] L. Petit, H. G. J. Eenink, M. Russ, W. I. L. Lawrie, N. W. Hendrickx, S. G. J. Philips, J. S. Clarke, L. M. K. Vandersypen, and M. Veldhorst, Nature **580**, 355 (2020).
[7] U. Güngördü and J. P. Kestner, Phys. Rev. B **99**, 081301 (2019).
[8] J. Yoneda, K. Takeda, T. Otsuka, T. Nakajima, M. R. Delbecq, G. Allison, T. Honda, T. Kodera, S. Oda, Y. Hoshi, et al., Nature Nanotechnology **13**, 102 (2018).
[9] K. W. Chan, W. Huang, C. H. Yang, J. C. C. Hwang, B. Hensen, T. Tanttu, F. E. Hudson, K. M. Itoh, A. Laucht, A. Morello, et al., Phys. Rev. Applied **10**, 044017 (2018).

Supplemental Material:
Microscopic bath effects on noise spectra in semiconductor quantum dots

Seongjin Ahn,[1] S. Das Sarma,[1] and J. P. Kestner[2,*]

[1] *Condensed Matter Theory Center and Joint Quantum Institute, Department of Physics, University of Maryland College Park, MD 20742, USA*

[2] *Department of Physics, University of Maryland Baltimore County, Baltimore, MD 21250, USA*

I. FITTING RESULTS

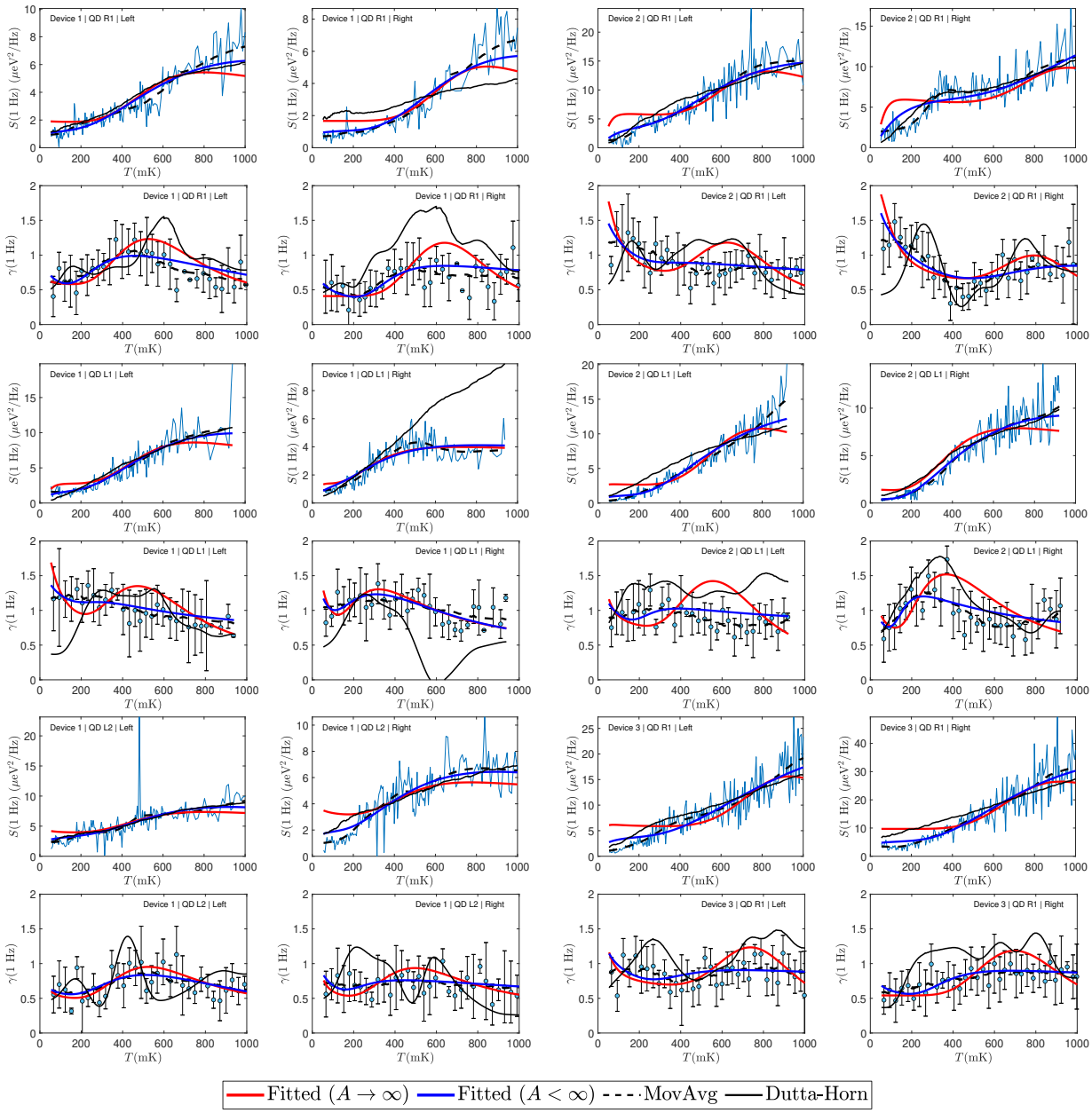

* jkestner@umbc.edu

FIG. 1: Fitting results using two fluctuators for S and γ along with the DH lines and measured data from Supplementary Fig. 2 of Ref. [1]

		Device 1 QD R1 Left		Device 1 QD R1 Right		Device 2 QD R1 Left		Device 2 QD R1 Right	
	Parameters	Fluctuator1	Fluctuator2	Fluctuator1	Fluctuator2	Fluctuator1	Fluctuator2	Fluctuator1	Fluctuator2
$A \to \infty$	τ (ms)	22.561	99.471	8.397	80.803	7.874	96.097	3.033	87.777
	E (meV)	0.134	3.120×10^{-4}	0.216	5.415×10^{-11}	0.215	6.770×10^{-3}	0.331	8.598×10^{-3}
	Δ^2 (meV^2)	2.850	1.636	2.688	1.644	2.718	2.027	1.832	2.372
$A < \infty$	τ (ms)	68.916	2.119	52.743	3.843×10^{-5}	41.06	5.743×10^{-6}	0.797	24.04
	E (meV)	3.353×10^{-3}	0.375	4.104×10^{-3}	1.518	0.040	1.986	0.729	0.049
	Δ^2 (meV^2)	1.559	7.999	1.529	21.899	2.482	29.722	8.807	3.909
	$\sqrt{A/\pi}$ (nm)	72.549		68.855		51.741		77.631	
		Device 1 QD L1 Left		Device 1 QD L1 Right		Device 2 QD L1 Left		Device 2 QD L1 Right	
$A \to \infty$	τ (ms)	105.924	24.400	102.331	66.145	10.921	111.491	42.183	103.979
	E (meV)	5.807×10^{-3}	0.122	3.401×10^{-3}	0.055	0.184	2.374×10^{-3}	0.082	1.589×10^{-3}
	Δ^2 (meV^2)	1.773	3.866	1.557	3.041	4.319	1.431	4.316	0.921
$A < \infty$	τ (ms)	1.183×10^{-3}	106.123	66.981	70.647	67.19	8.749×10^{-6}	0.05	60.142
	E (meV)	1.097	0.011	5.779×10^{-3}	0.052	0.018	2.443	0.803	9.176×10^{-3}
	Δ^2 (meV^2)	26.336	1.788	1.423	3.611	1.135	60.731	25.627	0.550
	$\sqrt{A/\pi}$ (nm)	60.220		203.41		36.858		47.645	
		Device 1 QD L2 Left		Device 1 QD L2 Right		Device 3 QD R1 Left		Device 3 QD R1 Right	
$A \to \infty$	τ (ms)	86.444	31.877	34.965	83.889	105.719	3.696	8.248	96.978
	E (meV)	8.874×10^{-4}	0.112	0.102	1.867×10^{-3}	2.664×10^{-3}	0.304	0.237	6.162×10^{-13}
	Δ^2 (meV^2)	1.852	1.421	1.352	1.856	1.878	3.011	2.658	1.732
$A < \infty$	τ (ms)	2.753	86.789	1.337×10^{-4}	44.339	51.53	3.498×10^{-5}	1.041×10^{-5}	77.322
	E (meV)	0.294	8.160×10^{-4}	1.332	0.014	0.034	3.295	2.645	3.707×10^{-3}
	Δ^2 (meV^2)	3.165	1.762	16.57	2.038	2.418	50.577	39.233	1.513
	$\sqrt{A/\pi}$ (nm)	100.802		49.852		29.501		38.835	

TABLE I: Fitting parameter values for Fig. 1

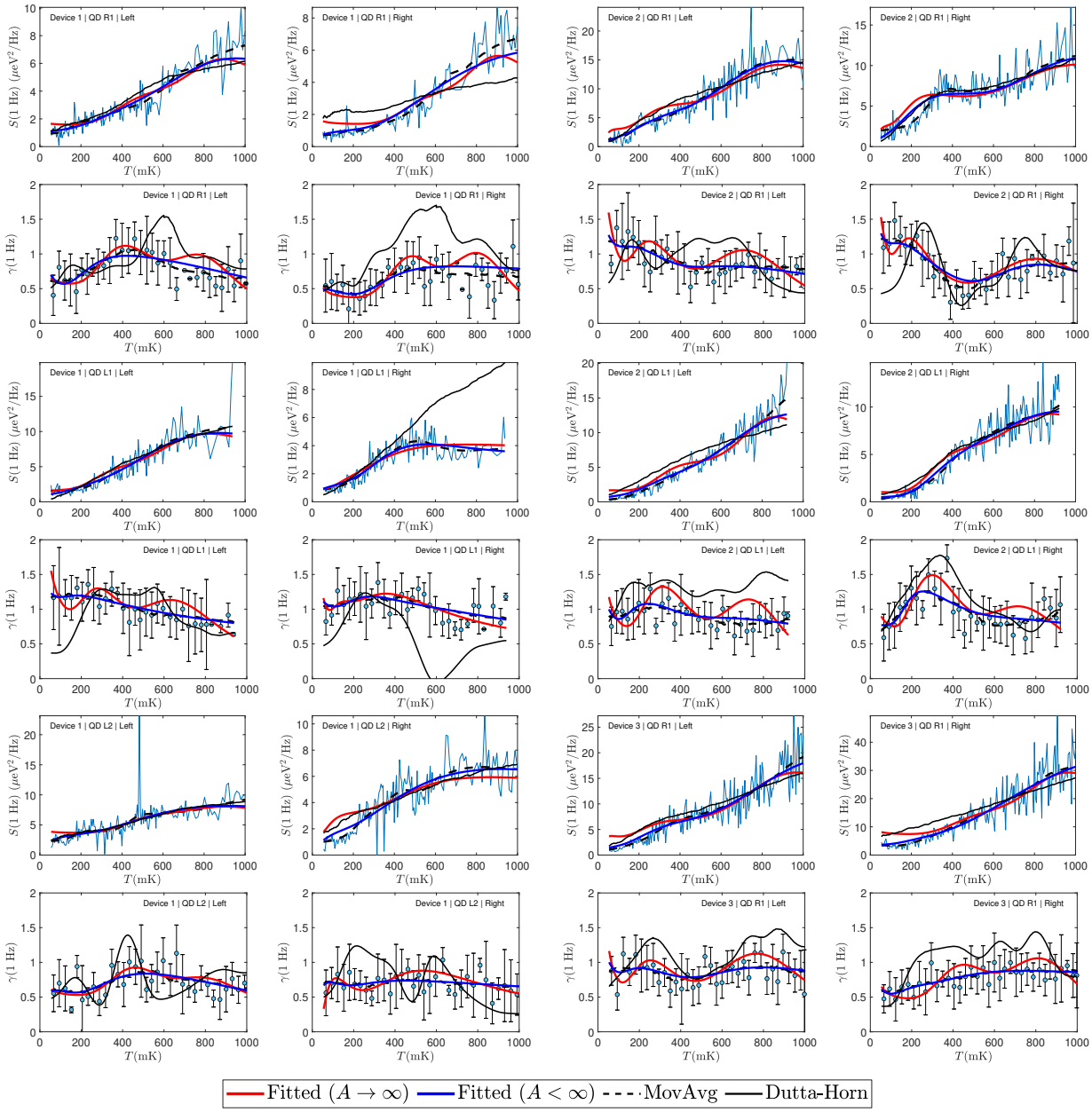

FIG. 2: Fitting results using three fluctuators for S and γ along with the DH lines and measured data from Supplementary Fig. 2 of Ref. [1]

		Device 1 QD R1 Left			Device 1 QD R1 Right		
	Parameters	Fluctuator1	Fluctuator2	Fluctuator3	Fluctuator1	Fluctuator2	Fluctuator3
$A \to \infty$	τ (ms)	1.414	15.557	94.933	71.026	0.747	4.466
	E (meV)	0.371	0.115	7.108×10^{-4}	1.223×10^{-3}	0.426	0.182
	Δ^2 (meV^2)	2.567	1.675	1.398	1.441	2.768	1.217
$A < \infty$	τ (ms)	52.697	21.100	6.023×10^{-6}	39.483	1.599×10^{-5}	4.933
	E (meV)	3.811×10^{-3}	0.120	1.484	0.035	2.013	6.278×10^{-6}
	Δ^2 (meV^2)	1.427	2.643	8.521	0.770	29.477	9.664
	$\sqrt{A/\pi}$ (nm)		126.656			50.487	
		Device 2 QD R1 Left			Device 2 QD R1 Right		
$A \to \infty$	τ (ms)	5.975	31.285	70.631	35.268	65.374	10.534
	E (meV)	0.256	0.056	6.637×10^{-3}	0.041	6.543×10^{-3}	0.246
	Δ^2 (meV^2)	2.993	1.589	1.040	1.737	0.996	2.225
$A < \infty$	τ (ms)	1.150×10^{-5}	3.354	55.618	6.734	42.332	0.644
	E (meV)	1.389	0.149	0.012	0.093	0.012	0.501
	Δ^2 (meV^2)	15.944	2.830	0.808	2.954	0.881	4.835
	$\sqrt{A/\pi}$ (nm)		115.063			153.980	
		Device 1 QD L1 Left			Device 1 QD L1 Right		
$A \to \infty$	τ (ms)	21.54	98.967	8.652	39.822	67.294	82.135
	E (meV)	0.074	5.084×10^{-3}	0.213	0.028	0.060	3.757×10^{-3}
	Δ^2 (meV^2)	1.921	1.098	3.967	0.780	3.199	1.034
$A < \infty$	τ (ms)	4.262	132.168	4.394×10^{-6}	115.430	4.180×10^{-6}	61.896
	E (meV)	0.179	2.983×10^{-3}	1.456	2.159×10^{-3}	0.747	0.068
	Δ^2 (meV^2)	3.243	1.145	21.435	1.442	6.751	2.536
	$\sqrt{A/\pi}$ (nm)		90.197			146.088	
		Device 2 QD L1 Left			Device 2 QD L1 Right		
$A \to \infty$	τ (ms)	1.352	19.094	89.447	105.672	18.485	5.352
	E (meV)	0.360	0.087	3.446×10^{-3}	1.406×10^{-3}	0.087	0.266
	Δ^2 (meV^2)	4.309	2.094	0.887	0.681	2.807	3.664
$A < \infty$	τ (ms)	3.906×10^{-6}	3.085	43.414	1.719×10^{-5}	123.117	0.279
	E (meV)	1.587	0.180	9.981×10^{-3}	1.458	5.633×10^{-5}	0.308
	Δ^2 (meV^2)	22.734	3.784	0.737	15.902	0.434	7.791
	$\sqrt{A/\pi}$ (nm)		111.874			121.981	
		Device 1 QD L2 Left			Device 1 QD L2 Right		
$A \to \infty$	τ (ms)	3.934	9.550	90.957	43.486	74.819	1.524
	E (meV)	0.306	0.142	7.093×10^{-4}	0.100	0.015	2.346×10^{-8}
	Δ^2 (meV^2)	1.128	1.050	1.703	1.539	0.882	39.844
$A < \infty$	τ (ms)	17.511	1.020	1.874	1.423×10^{-5}	0.020	15.484
	E (meV)	6.693×10^{-3}	0.115	0.344	1.621	2.075×10^{-8}	0.08
	Δ^2 (meV^2)	2.476	2.064	4.947	18.161	2046.936	1.851
	$\sqrt{A/\pi}$ (nm)		84.974			49.926	
		Device 3 QD R1 Left			Device 3 QD R1 Right		
$A \to \infty$	τ (ms)	68.903	36.885	5.639	11.055	1.820	81.042
	e	4.674×10^{-3}	0.052	0.284	0.135	0.378	1.444×10^{-3}
	c	1.138	1.153	3.235	1.094	2.835	1.380
$A < \infty$	τ (ms)	2.157×10^{-3}	41.875	0.198	0.158	7.727×10^{-6}	42.739
	e	1.204	0.012	0.291	0.498	2.397	7.674×10^{-3}
	c	16.261	0.907	4.344	3.359	32.221	1.319
	$\sqrt{A/\pi}$ (nm)		95.321			52.171	

TABLE II: Fitting parameter values for Fig. 2

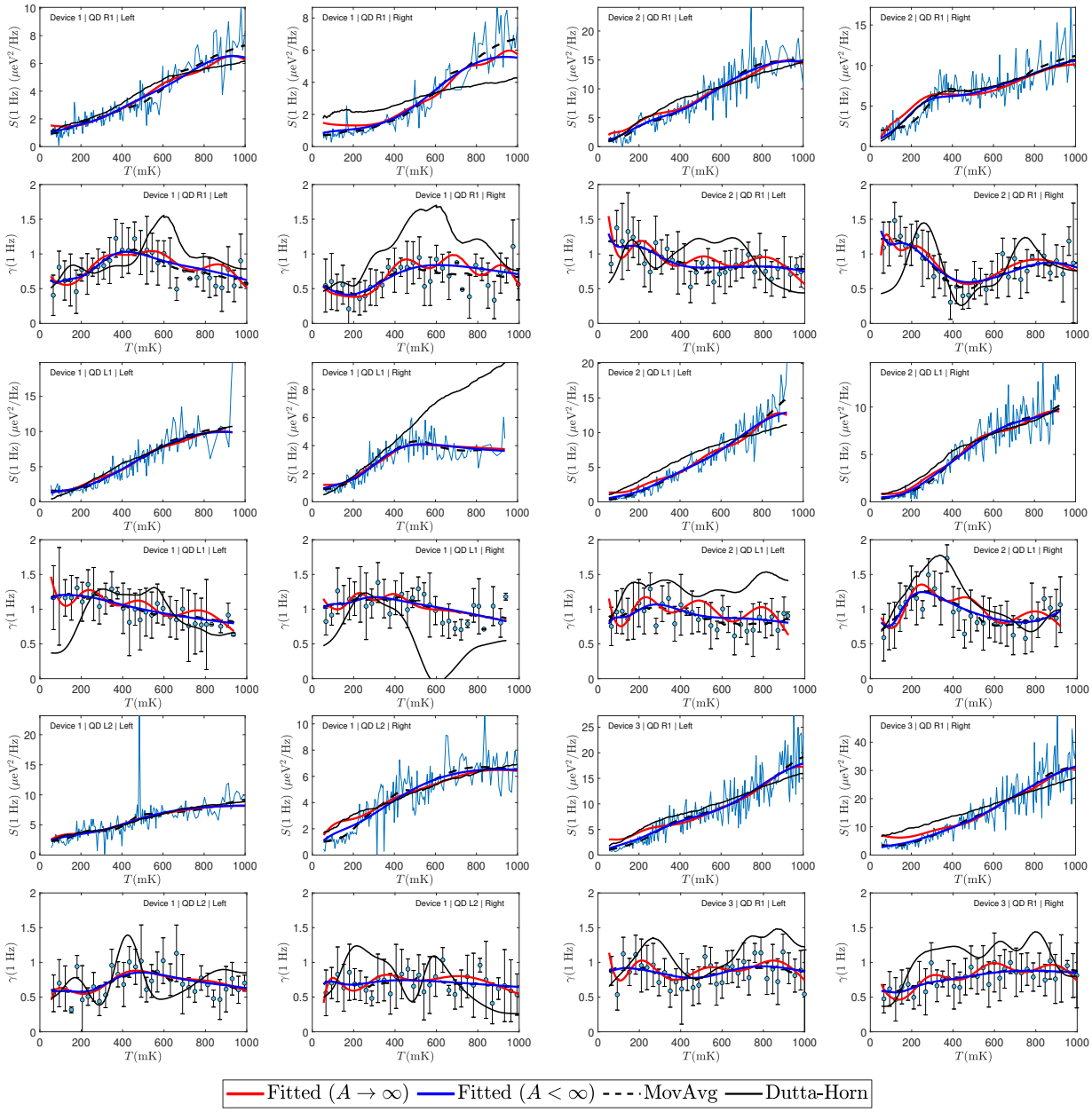

FIG. 3: Fitting results using four fluctuators for S and γ along with the DH lines and measured data from Supplementary Fig. 2 of Ref. [1]

		Device 1 QD R1 Left				Device 1 QD R1 Right			
	Parameters	Fluctuator1	Fluctuator2	Fluctuator3	Fluctuator4	Fluctuator1	Fluctuator2	Fluctuator3	Fluctuator4
$A \to \infty$	τ (ms)	2.422	0.151	87.038	23.495	0.119	2.967	71.166	7.938×10^{-3}
	E (meV)	0.246	0.577	1.218×10^{-3}	0.081	0.473	0.186	1.368×10^{-3}	0.837
	Δ^2 (meV^2)	1.773	2.453	1.286	0.974	2.084	0.980	1.332	2.563
$A < \infty$	τ (ms)	6.220	2.492×10^{-5}	0.974	15.794	8.062×10^{-6}	23.28	36.558	0.749
	E (meV)	0.173	1.351	0.099	8.073×10^{-3}	1.477	1.482×10^{-3}	0.018	0.331
	Δ^2 (meV^2)	3.361	8.325	1.287	1.704	13.456	1.561	0.547	2.050
	$\sqrt{A/\pi}$ (nm)	168.335				105.693			
		Device 2 QD R1 Left				Device 2 QD R1 Right			
$A \to \infty$	τ (ms)	2.371	1.846	29.716	69.735	12.739	58.062	25.659	0.990
	E (meV)	0.220	0.366	0.049	6.351×10^{-3}	0.233	0.014	0.055	8.509×10^{-5}
	Δ^2 (meV^2)	1.461	3.105	1.274	0.837	2.327	0.959	1.506	18.799
$A < \infty$	τ (ms)	3.428×10^{-6}	18.303	2.379×10^{-3}	15.052	46.131	2.572×10^{-5}	6.020	0.182
	E (meV)	1.130	0.021	1.042	0.077	0.011	0.920	0.090	0.626
	Δ^2 (meV^2)	8.087	0.848	6.958	2.044	0.773	3.211	2.643	4.615
	$\sqrt{A/\pi}$ (nm)	156.292				190.390			
		Device 1 QD L1 Left				Device 1 QD L1 Right			
$A \to \infty$	τ (ms)	2.802	23.609	2.051	105.68	6.418	136.169	2.272	48.665
	E (meV)	0.320	0.061	0.217	4.242×10^{-3}	0.080	1.420×10^{-3}	0.170	0.094
	Δ^2 (meV^2)	3.888	1.394	2.145	0.954	0.937	1.370	1.296	2.367
$A < \infty$	τ (ms)	3.070×10^{-6}	0.020	54.406	5.877×10^{-6}	0.158	2.349×10^{-5}	64.417	29.174
	E (meV)	0.159	0.571	0.035	1.599	0.027	0.636	0.069	0.025
	Δ^2 (meV^2)	9.644	8.706	1.567	18.261	4.153	5.562	3.344	1.454
	$\sqrt{A/\pi}$ (nm)	84.123				167.154			
		Device 2 QD L1 Left				Device 2 QD L1 Right			
$A \to \infty$	τ (ms)	0.260	23.27	2.816	74.646	96.990	17.379	2.710	1.703
	E (meV)	0.497	0.058	0.210	4.174×10^{-3}	1.712×10^{-3}	0.070	0.202	0.366
	Δ^2 (meV^2)	4.403	1.080	2.323	0.717	0.572	1.421	2.652	3.941
$A < \infty$	τ (ms)	3.112×10^{-6}	1.064	17.741	7.982×10^{-3}	2.944	5.225×10^{-6}	0.122	82.719
	E (meV)	1.610	0.245	0.040	2.614×10^{-5}	0.177	1.224	1.096	2.093×10^{-3}
	Δ^2 (meV^2)	21.912	4.560	0.690	1428.275	4.416	11.395	45.573	0.449
	$\sqrt{A/\pi}$ (nm)	123.312				134.806			
		Device 1 QD L2 Left				Device 1 QD L2 Right			
$A \to \infty$	τ (ms)	110.546	3.693	10.571	18.448	17.298	64.598	15.684	1.688
	E (meV)	9.377×10^{-3}	3.997×10^{-12}	0.246	0.116	0.092	0.014	0.194	2.136×10^{-5}
	Δ^2 (meV^2)	0.653	17.251	1.073	1.088	0.932	0.724	1.598	29.137
$A < \infty$	τ (ms)	20.559	53.534	11.689	10.393	13.526	1.393×10^{-4}	2.469×10^{-7}	8.345
	E (meV)	0.038	2.170×10^{-3}	0.146	0.289	0.081	1.351	8.083×10^{-3}	1.200×10^{-10}
	Δ^2 (meV^2)	0.552	1.402	1.768	1.336	1.914	15.242	0.151	4.731
	$\sqrt{A/\pi}$ (nm)	209.489				52.668			
		Device 3 QD R1 Left				Device 3 QD R1 Right			
$A \to \infty$	τ (ms)	29.569	66.689	5.789	1.180	1.889	69.086	18.54	0.544
	E (meV)	0.048	4.705×10^{-3}	0.191	0.426	0.270	2.393×10^{-3}	0.079	0.495
	Δ^2 (meV^2)	0.926	0.931	1.258	3.286	1.458	1.166	0.624	2.918
$A < \infty$	τ (ms)	3.478×10^{-3}	41.659	12.827	2.163×10^{-5}	33.257	10.44	3.095×10^{-5}	4.566×10^{-3}
	E (meV)	1.062	7.116×10^{-3}	0.074	0.774	0.03	3.924×10^{-4}	1.853	0.671
	Δ^2 (meV^2)	12.955	0.675	1.148	5.520	0.627	2.543	21.909	5.240
	$\sqrt{A/\pi}$ (nm)	118.107				73.297			

TABLE III: Fitting parameter values for Fig. 3

II. TRUNCATED TEMPERATURE DISTRIBUTION

We now rederive a modified version of Eq. 8 of the main text, starting from Eq. 4, using a truncated gaussian distribution to avoid including negative temperatures.

$$S(\omega) = \frac{2\Delta^2}{\omega\sqrt{\pi/2}\sigma_{sb}\left(1+\mathrm{erf}\left(\frac{T}{\sqrt{2}\sigma_{sb}}\right)\right)}\int_0^\infty dT_{sb} e^{-\frac{(T_{sb}-T)^2}{2\sigma_{sb}^2}} \mathrm{sech}\left(\frac{E}{k_B}\left(\frac{1}{T_{sb}}-\frac{1}{T_\omega}\right)\right)$$

$$\approx \frac{2\Delta^2}{\omega}\mathrm{sech}\left(\frac{E}{k_B}\left(\frac{1}{T}-\frac{1}{T_\omega}\right)\right) + \frac{2\Delta^2}{\omega}\frac{\sigma_\omega}{\sqrt{\sigma_{sb}^2+\sigma_\omega^2}}\frac{1+\mathrm{erf}\left(\frac{\sigma_{sb}^2 T_\omega+\sigma_\omega^2 T}{\sqrt{2}\sigma_{sb}\sigma\omega\sqrt{\sigma_{sb}^2+\sigma_\omega^2}}\right)}{1+\mathrm{erf}\left(\frac{T}{\sqrt{2}\sigma_{sb}}\right)} e^{-\frac{(T-T_\omega)^2}{2(\sigma_{sb}^2+\sigma_\omega^2)}}, \quad (1)$$

assuming well-separated peaks at T and T_ω as before. In the low-frequency limit $T_\omega \ll T$ and $\sigma_\omega \ll \sigma_{sb}$,

$$S(\omega) \approx \frac{4\tau\Delta^2}{1+\omega^2\tau^2} + \frac{2E\Delta^2}{k_B\sigma_{sb}\omega\ln^2\frac{1}{\omega\tau}}\frac{2e^{-\frac{(T-T_\omega)^2}{2\sigma_{sb}^2}}}{1+\mathrm{erf}\left(\frac{T}{\sqrt{2}\sigma_{sb}}\right)}. \quad (2)$$

This reduces to Eq. 8 of the main text when the erf function is unity.

[1] E. J. Connors, J. Nelson, H. Qiao, L. F. Edge, and J. M. Nichol, Phys. Rev. B **100**, 165305 (2019).